Desalination and Water Treatment
www.deswater.com
doi: 10.1080/19443994.2014.987178

57 (2016) 3642–3653
February

Taylor & Francis
Taylor & Francis Group

Assessment of Pb^{2+} ions removal efficiency of nanomagnetite-loaded poly (acrylamide-co-acrylic acid) hydrogel in fixed-bed microcolumn from aqueous solution

Neeraj Sharma, Alka Tiwari*

Department of Chemistry, Govt. V.Y.T. PG. Autonomous College, Durg, Chattishgarh 491001, India, Tel. +91 9098190861; email: neeraj.sharma.shyam@gmail.com (N. Sharma), Tel. +91 7415514000; Fax: +91 788 2324783; emails: brnsbarc18@gmail.com, alkatiwari18@yahoo.co.in (A. Tiwari)

Received 7 July 2014; Accepted 2 November 2014

ABSTRACT

The adsorption potential of nanomagnetite-loaded poly (acrylamide-co-acrylic acid) hydrogel, to remove Pb(II) ions from aqueous solution as well as contaminated water, was investigated using fixed-bed adsorption column. The effect of inlet Pb(II) concentration, feed flow rate, and bed depth on the breakthrough characteristics of the adsorption system were determined. The adsorption capacity increased with the increase in initial Pb(II) concentration and flow rate, but decreased with increasing bed depth. The Thomas, Yoon–Nelson, and Adams–Bohart kinetic models were applied to the experimental data to predict the breakthrough curves and to determine the characteristic parameters of the column, useful for process design.

Keywords: Adsorption; Fixed-bed column technology; Kinetic; Modeling; Breakthrough curves

1. Introduction

The occurrence of toxic heavy metal ions in natural water resources is one of the major environmental concerns in both the public and regulatory sphere for preventing water pollution because of their toxicity and threat to human life [1,2]. Being non-biodegradable and likely to accumulate in living tissues, toxic metal ions cause various diseases and disorders [3].

Lead is an industrial pollutant, which enters the ecosystem through the industrial waste effluents particularly from electroplating metal finishing, battery manufacturing, and chemical manufacturing industries. Lead is extremely toxic to human beings. The presence of lead in drinking water beyond the permissible limit (0.05 mg dm^{-3}) may cause adverse health effects such as encephalopathy, hepatitis, anemia, nephritic syndrome, mental retardation, headache, dizziness, irritability, and weakness of muscles [4]. Lead (II) forms complexes with oxo groups in enzymes to affect, virtually, all steps involved in the process of hemoglobin synthesis and porphyrin metabolism [5]. Lead poisoning may cause accumulative poisoning, cancer, liver, kidney, reproductive system, and brain damages when found above the tolerance level [6]. Therefore, it is very necessary that lead should be removed from wastewater before being discharged into an aquatic environment for protecting all the living resources.

*Corresponding author.

Numerous conventional processes exist for the removal of toxic heavy metal pollutants from aquatic system, including precipitation, electroplating, chemical coagulation, ion-exchange, membrane separation, and adsorption [7–9]. However, most of the methods are not economically feasible as well as not eco-friendly in nature. In this context, there has been a great deal of research into finding eco-friendly, cost-effective methods for the removal of toxic heavy metal ions from wastewater. Adsorption is a worthy economical and effective process and is eco-friendly [10]. In recent years, considerable attention has been devoted to the study of removal of toxic heavy metal ions from aquatic system by sorption using insoluble polymeric hydrogel sorbents having different functional groups that can be complexed with metal cations from aqueous solutions [11,12]. The main advantages of such polymeric hydrogels are easy loading and, in most cases, stripping of cations with simple chemicals, reusability, and the possibility of semi-continuous operation. The sorption of toxic metal ions by copolymeric sorbents depends on various macromolecular characteristics like the hydrophilic/hydrophobic balance of matrix, extent of cross-linking, the structure of the attached ligand function, and the stability constants related to the resulting copolymer–metal complex [13–15].

In this present work, we explore the novel sorbent nanomagnetite-loaded poly (acrylamide-co-acrylic acid) hydrogel (nanomagnetite-loaded PAA hydrogel) which has a high affinity for Pb(II) ions and fully exploits its ability in a wide range of metal concentrations. The efficient removal of lead ions by the sorbent was studied as a function of different bed depths, flow rates, and inlet Pb(II) concentrations in a fixed-bed column system. This study has applied empirical models by Thomas, Yoon–Nelson, and Adams–Bohart for describing lead removal from aqueous solution on a fixed-bed of nanomagnetite-loaded PAA hydrogel.

In order to compare the adsorption capacity of PAA hydrogel with and without nanomagnetite impregnation, the same column experiments were performed which showed percentage removal of Pb(II) ions as 98.92 and 79.25%, respectively. Thus, it was observed that the encapsulated nanomagnetite particles improved the adsorption capacity of the above magnetic co-polymer.

2. Materials and methods

2.1. Material

The monomer acrylamide, N,N´-methylene bis acrylamide (cross-linker), potassium per sulphate (initiator), sodium hydroxide pellets, anhydrous ferric chloride, and ferrous chloride tetra hydrate were purchased from Molychem, Mumbai, India. Acrylic acid was purchased from Himedia, Mumbai, India. Triple-distilled water was used throughout the experiments.

2.2. Synthesis of nanomagnetite-loaded PAA hydrogel

To a mixture of acrylamide and acrylic acid (1:1 ratio) the cross-linker (N,N´-methylene-bis-acrylamide) and initiator (potassium per sulfate) were added and heated at 70˚C in an electric oven for 1 h. The copolymeric hydrogel so formed was washed with distilled water and cut into small uniform pieces. For *in situ* magnetization, these pieces were equilibrated in an aqueous solution of ferrous chloride and ferric chloride for 24 h. The Fe^{3+}/Fe^{2+}-loaded pieces of copolymer were then added into conc. ammonia solution and kept overnight. The magnetic hydrogel was then washed thoroughly with distilled water, dried, and crushed into a fine powder.

2.3. Characterization of nano-magnetite-loaded PAA hydrogel

The adsorbent—"Nano Magnetite Loaded PAA Hydrogel" was characterized by XRD, Fourier transform infrared spectroscopy (FTIR), AFM, and TEM analysis.

2.3.1. XRD analysis

The crystalline nature of the nanomagnetite-loaded PAA hydrogel was studied on a Bruker D8 advanced X-ray diffractometer with scanning range of 20˚–80˚ (2θ) using Cu Kα radiation with a wavelength of 1.5406 Å (UGC-DAE, Indore, India).

2.3.2. FTIR analysis

FTIR spectra of adsorbent were recorded using Varian Vertex FTIR Spectrometer (UGC-DAE, Indore, India).

2.3.3. AFM analysis

The morphology and diameter of magnetite nanoparticles was examined by contact mode AFM (NS-E, Digital Instrument Inc, USA) using silicon nitrate tip. The sample was prepared for AFM analysis by placing a few drops of the suspension of Fe_3O_4 in 50% HCl on a cleaved mica sheet (UGC-DAE, Indore, India).

2.3.4. TEM analysis

The average particle size, size distribution, and morphology of iron oxide nanoparticles were examined using a TECNAI—G20 TEM at a voltage of 200 kV. The solvent dispersion of the particles was drop-cast onto a carbon-coated copper grid and the grid was air dried at ambient conditions (25 ± 1°C) before loading into the microscope (AIIMS, New Delhi, India).

2.4. Preparation of stock solution

The synthetic solutions were prepared by diluting Pb(II) standard solution (concentration 1,000 mg dm^{-3}) obtained by dissolving 0.160 g of Pb $(NO_3)_2$ in 100 ml distilled water. Fresh dilutions were used in each experiment.

2.5. Analytical technique

The concentration of Pb(II) ions was determined using atomic absorption spectrometer (Varian AA-24-OFS) and each experiment was carried out in triplicate under identical conditions to get the mean values.

2.6. Fixed-bed adsorption microcolumn study

Fixed-bed adsorption studies were conducted in a microcolumn made of polyethylene having an inner diameter of 0.5 cm and a height of 10 cm, at a constant temperature of 25°C. The column was packed with different bed heights of nanomagnetite-loaded PAA hydrogel on a glasswool support. The results of batch experiment showed that the maximum adsorption of Pb(II) ions was at pH 4, [16] hence all column experiments were carried out at pH 4. A known concentration of lead solution was allowed to pass through the bed at a constant flow rate (1 ml min^{-1}) in a down-flow manner. The lead solution was then collected at different time intervals until the column got exhausted and the concentration of Pb(II) ions was determined by atomic absorption spectrometer. The important design parameters such as column bed height, flow rate of metal solution into column, and initial metal ion concentration have been investigated.

2.7. Analysis of column data

The efficiency of the column was evaluated by determining breakthrough curves. The time for breakthrough appearance and the shape of the breakthrough curves are very important characteristics for determining the operation and the dynamic response of adsorption column. The breakthrough curves show the loading behavior of Pb(II) ions to be removed from solution in a fixed bed and is usually expressed in terms of adsorbed metal concentration (C_{ad} = inlet metal concentration and (C_0)—outlet metal concentration (C_t)) or normalized concentration defined as the ratio of effluent metal concentration to inlet metal concentration (C_t/C_0) as a function of time or volume of effluent for a given bed height [17]. The breakthrough time t_B is defined as the time required for the concentration of metal ions in the effluent to reach 5% of the applied concentration. The exhaustion time t_E is defined as the time when the concentration of metal ions in the effluent becomes 90% of the applied concentration. The breakthrough volumes V_B and exhaustion volumes V_E are the effluent volumes at breakthrough time and exhaustion time, respectively. Effluent volume (V_{eff}) can be calculated from the following equation:

$$V_{eff} = Qt_{total} \tag{1}$$

where t_{total} and Q are the total flow time (min) and volumetric flow rate (ml min^{-1}), respectively. The area under the breakthrough curve (A) obtained by integrating the adsorbed concentration (C_{ad}; mg dm^{-3}) vs. t (min) plot can be used to find the total adsorbed metal quantity (maximum column capacity). Total adsorbed metal quantity (q_{total}; mg g^{-1}) in the column for a given feed concentration and flow rate (Q) is calculated from the following equation:

$$Q_{total} = \frac{Q \cdot (C_0 - C_t) \cdot t_{total}}{1,000} \tag{2}$$

Total amount of metal ions sent to column (m_{total}) is calculated from the following equation:

$$m_{total} = \frac{C_0 \cdot Q \cdot t_{total}}{1,000} \tag{3}$$

Total removal percent of Pb(II) is the ratio of the maximum capacity of the column (q_{total}) to the total amount of Pb(II) sent to column (m_{total}) from the following equation:

$$\text{Total removal}\,(\%) = \frac{q_{total}}{m_{total}} \times 100 \tag{4}$$

Equilibrium metal uptake (q_{eq}) (or maximum capacity of the column) in the column is defined by Eq. (5) as

the total amount of metal sorbed (q_{total}) per gram of sorbent (X) at the end of the total flow time:

$$q_{eq} = \frac{q_{total}}{X} \tag{5}$$

2.8. Modeling of column dynamics

The sorption performance of the Pb(II) through the column was analyzed by bed depth service time model (BDST), Thomas, Yoon–Nelson, and Bohart–Adams models by starting at concentration ratio, C_t/C_0 = breakthrough point until $C_t/C_0 > 0.90$ that is 90% breakthrough for lead by considering the safe water-quality standards and operating limits of mass transfer zone of a column.

2.9. BDST model

BDST is a simple model, which states that bed depth (Z) and service time (t) of a column bears a linear relationship. The linearized form of the model is given by the following equation:

$$t = \frac{N_0 Z}{C_0 Q} - \frac{1}{K_a C_0} \ln\left(\frac{C_0}{C_t} - 1\right) \tag{6}$$

where C_t is the breakthrough metal ion concentration (mg dm^{-3}), N_0 the sorption capacity of bed (mg l^{-1}), Q the flow rate (ml min^{-1}), and K_a is the rate constant (l mg^{-1} min^{-1}).

2.10. Thomas model

The Thomas model is one of the most general and widely used models. The model is applicable in the system with a constant flow rate and no axial dispersion, and its behavior matches the Langmuir isotherm and the second-order reversible reaction kinetics. The linearized form of the model is given by the following equation.

$$\ln\left(\frac{C_0}{C_t} - 1\right) = \frac{K_{Th} q_0 M}{Q} - \frac{K_{Th} C_0}{Q} V \tag{7}$$

In this expression, k_{Th} (ml mg^{-1} min^{-1}) is the Thomas rate constant, q_0 (mg g^{-1}) is the equilibrium adsorbate uptake, Q (ml min^{-1}) is the flow rate, and V (ml) is the effluent volume. C_t is the concentration of metal ion at time t and C_0 is the initial metal ion concentration.

2.11. Yoon–Nelson model

A simple theoretical model developed by Yoon–Nelson was applied to investigate the breakthrough behavior of Pb(II) ions on nano-iron oxide-loaded PAA hydrogel. This model is based on the assumption that the increase in rate or decrease in the probability of adsorption for each adsorbate molecule is proportional to the probability of adsorbate adsorption and the probability of adsorbate breakthrough on the adsorbent. The Yoon–Nelson model not only is less complicated than other models but also requires no detailed data concerning the characteristics of adsorbate, the type of adsorbent, and the physical properties of adsorption bed. The linearized model for a single-component system is expressed by the following equation.

$$\ln\left(\frac{C_t}{C_0 - C_t}\right) = K_{YN} t - \tau \cdot K_{YN} \tag{8}$$

where k_{YN} (min^{-1}) is the Yoon–Nelson rate constant, τ is the time required for 50% adsorbate breakthrough (min), and t is the sampling time (min). C_t is the concentration of metal ion at time t and C_0 is the initial metal ion concentration.

For a given bed:

$$q_{0YN} = \frac{C_0 \cdot Q \cdot \tau}{1,000\, X} \tag{9}$$

where q_{0YN} is the adsorption capacity, C_0 is the initial metal ion concentration, Q is the flow rate, X is the weight of adsorbent, and τ is the 50% breakthrough time.

2.12. Adams–Bohart model

This model was established based on the surface reaction theory and it is assumed that equilibrium is not instantaneous. Therefore, the rate of adsorption was proportional to both the residual capacity of the adsorbent and the concentration of the sorbing species. The mathematical equation of the model can be written as:

$$\ln\left(\frac{C_t}{C_0}\right) = K_{AB} \cdot C_0 \cdot t - K_{AB} \cdot q_{AB} \cdot \frac{Z}{Q} \tag{10}$$

where C_0 and C_t are the inlet and outlet adsorbate concentrations (mg dm^{-3}), respectively, K_{AB} is the rate constant (l mg^{-1} min^{-1}), q_{AB} is the removal capacity

(mg l^{-1}), Z (cm) is the bed depth, Q is the linear flow velocity (ml min^{-1}), and t is the service time (min).

Value of removal capacity q in mg g^{-1} is calculated as follows:

$$q = \frac{q_{AB} \cdot BV_s}{m} \tag{11}$$

where q is the removal capacity (mg g^{-1}), BVs is the fixed bed volume (L), and m is mass of the bed (g).

2.13. Column desorption study

Column desorption study was carried out after the column adsorption studies were conducted, at 25 ± 0.2°C, using 0.1 M HNO_3 solution at a flow rate of 1 ml min^{-1} and 1 cm bed depth to provide sufficient exchangeable H^+ ions for 4 h and then washed with hot distilled water and could be reused for further adsorption experiment.

3. Results and discussion

3.1. Characterization of nanomagnetite-loaded PAA hydrogel

The nanomagnetite-loaded PAA hydrogel was synthesized and characterized by the following instrumental methods.

3.1.1. XRD analysis

The XRD pattern of nanomagnetite-loaded PAA hydrogel showed five characteristic peaks ($2\theta = 30.09$, 35.44, 43.07, 56.96, and 62.55), marked by their indices [(511), (311), (400), (511), and (440)]. The position and relative intensities of all diffraction peaks in Fig. 1 match well with those from the JCPDS file No. 89–5,984 for magnetite (Fe_3O_4) and reveal that the prominent phase formed is Fe_3O_4 with resultant nanoparticles of pure magnetite with cubic structure. Magnetite particles are obtained according to the reaction:

$$2FeCl_3 + FeCl_2 + 8NH_4OH \longrightarrow Fe_3O_4 + 8NH_4Cl + 4H_2O$$

3.1.2. FTIR analysis

FTIR of nanomagnetite-loaded PAA hydrogel as shown in Fig. 2, indicated the band at 2,930.55 cm^{-1}, assigned to C–H bond of methylene group. The FTIR analysis indicated the band due to acrylamide at 3,400,

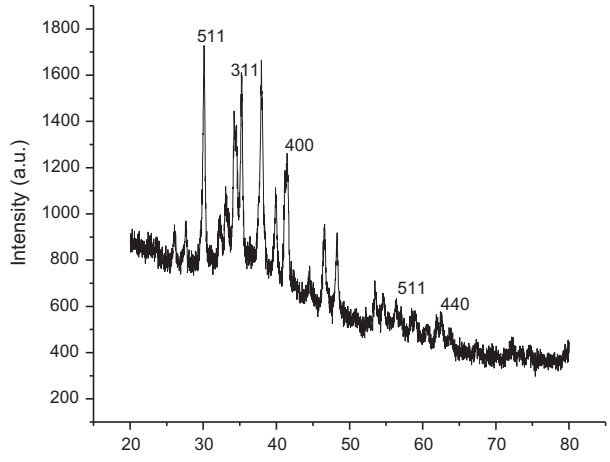

Fig. 1. XRD pattern of nanomagnetite-loaded PAA hydrogel.

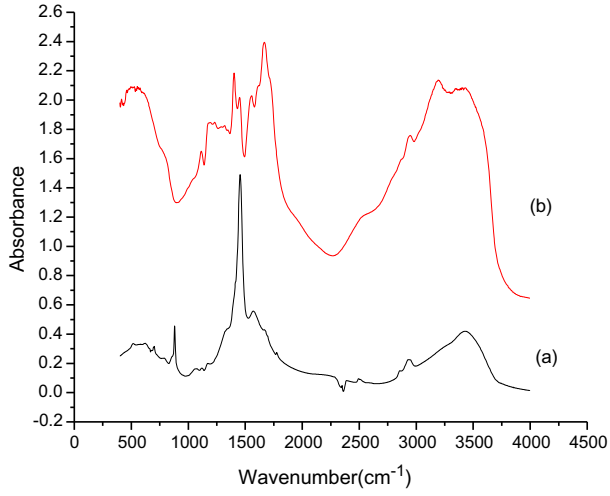

Fig. 2. FTIR pattern of (a) nanomagnetite-loaded PAA hydrogel before sorption of Pb(II) ions. (b) Nanomagnetite-loaded PAA hydrogel after sorption of Pb(II) ions.

1,646, 1,549, and 1,411 cm^{-1} attributed to N–H stretching, C=O stretching, N–H bending, and C–N stretching, respectively, which are the characteristics of the amide ($CONH_2$) group. Absorption peaks due to acrylic acid were observed at 1,725 and 1,449 cm^{-1} due to C=O and C–O stretching of the carboxylic (–COOH) group, and at 3,446.24 cm^{-1} due to –OH stretching of –COOH group. The characteristic peak at 566.69 cm^{-1} relates to Fe–O group, which indicates the loading of nano-iron oxide particles on PAA hydrogel because the surface of iron oxide with negative charges has an affinity toward PAA hydrogel, the magnetite nanoparticles could be loaded into protonated copolymer by the electrostatic interaction and chemical reaction

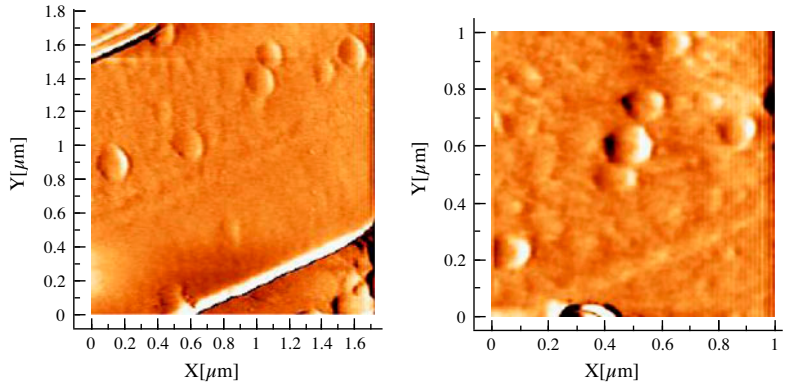

Fig. 3. AFM topographic images of magnetic nanoparticles on mica.

through N,N´-methylene-bis-acrylamide cross-linking. In Fig. 2(b), a slight change in shape and intensity of absorbance (due to $–CONH_2$ and –COOH groups) has been noticed which indicates that electron-rich nitrogen of amide group of acrylamide moiety and $–COO^-$ group of acrylic acid moiety involve in the removal of Pb(II) ions. Change in the peak position and intensity for Fe–O group stretching from 566.69 to 551 cm^{-1} indicates that Pb(II) ions coordinate with electron-rich oxygen of magnetite nanoparticles (Fe_3O_4).

3.1.3. AFM analysis

The morphology of the magnetite nanoparticles, using contact mode AFM, was found to be spherical, having size distribution in two different diameter (height) ranges of 10–20 nm (mean height: 15 nm) and 40–110 nm (mean height: 50 and 80 nm) as shown in Fig. 3. However, some larger particle size in figure may be a result of agglomeration of smaller magnetite nanoparticles in order to reduce the inherent large surface energies for magnetite nanoparticles.

3.1.4. TEM analysis

The shape, size, and morphology of iron oxide nanoparticles were determined through TEM imaging. The TEM images of nanoparticles show almost cubic iron oxide particles with an average size of less than 10 nm, as shown in Fig. 4. Size of these nanoparticles lie within the range of 1–9 nm. It should be noted, however, that the majority of the particles were scattered, a few of them showing aggregates indicate stabilization of the nanoparticles. The results represented by TEM images concluded that the particle size of individual nanoparticles seem to be 1–10 nm, whereas majority of nanoparticles exhibit smaller sizes, i.e. 5 and 8 nm.

3.2. Column studies of adsorption of Pb(II) ions onto nanomagnetite-loaded PAA hydrogel

Several operational factors such as bed depth (Z), flow rate (Q), and initial adsorbate concentration (C_0) affect the shape of a breakthrough curve and

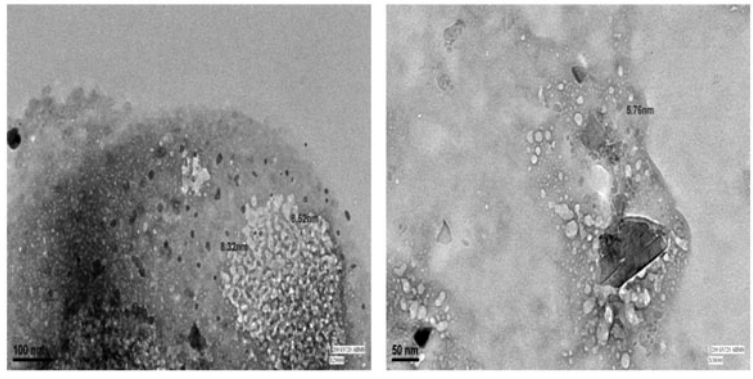

Fig. 4. Transmission electron micrograph of iron oxide nanoparticles.

maximum capacity of the column. In this study, the effect of these parameters on breakthrough curve and maximum capacity of the column was investigated.

3.2.1. Effect of bed depth

The breakthrough curve for Pb(II) adsorption for three different bed depths (0.25, 0.5, and 1 cm) at constant adsorbate feed flow rate (1 ml min^{-1}) and adsorbate inlet concentration (10 mg dm^{-3}) is shown in Fig. 5. It was noticed that both the breakthrough time and exhaustion time showed an increase with increasing bed depth. A higher uptake was observed at higher bed height due to the increase in the specific surface area of the adsorbent, which provides more fixation of the Pb(II) ions with more binding sites for the adsorption process to proceed. The increase in bed depth would increase the mass transfer zone. The mass transfer zone in a column moves from the entrance of the bed and proceeds toward the exit. Hence, for the same influent concentration and fixed-flow rate, an increase in bed depth would create a longer distance for the mass transfer zone to reach the exit, subsequently resulting in an extended breakthrough time. For higher bed depth, the increase in adsorbent mass would provide a larger service area leading to an increase in the volume of treated solution [18]. Also an increase in the maximum bed adsorption capacity (q_0) was noticed at the breakthrough point with the increase in bed depth. The values are given in Table 1.

3.2.2. Effect of flow rate

The effect of feed flow rate on the adsorption of Pb(II) ions on nano-iron oxide-loaded PAA hydrogel was investigated by varying the feed flow rate (1, 2, and 3 ml min^{-1}) at a constant adsorbent bed depth of 1 cm and inlet adsorbate concentration of 10 mg dm^{-3}, as shown by the breakthrough curve in Fig. 6. The trend of the curves showed that at higher flow rate, the front of the adsorption zone quickly reached the top of the column. This implies that the column was saturated early. Lower flow rate resulted in longer contact time, as well as a shallow adsorption zone. Relatively early breakthrough and exhaustion time were observed for higher flow rates with steeper curve; resulting in less adsorption uptake [19] (Table 2).

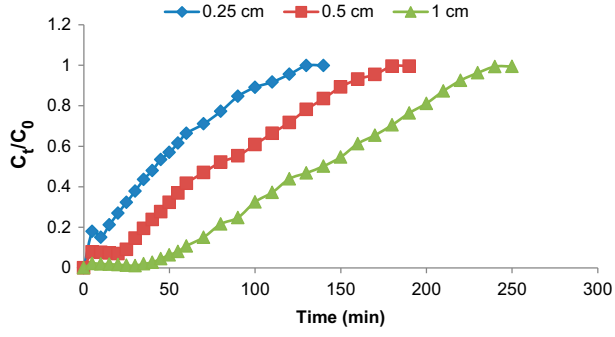

Fig. 5. The effect of bed depth on breakthrough curve at temperature = 25 ± 0.2°C, pH 4, bed depth of nanomagnetite-loaded PAA hydrogel = 0.25, 0.5 and 1 cm, flow rate = 1 ml min^{-1}, and Pb(II) initial concentration = 10 mg dm^{-1}.

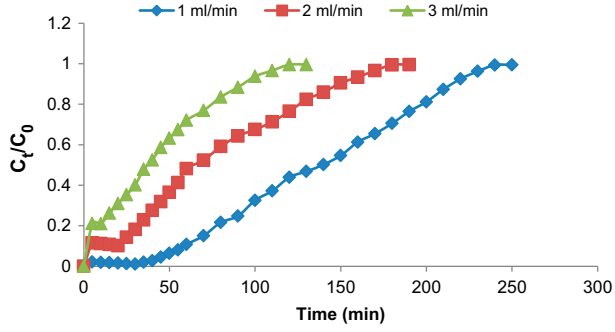

Fig. 6. The effect of flow rate on breakthrough curve at temperature = 25 ± 0.2°C, pH 4, flow rate = 1, 2, and 3 ml min^{-1}, bed height = 1 cm, and Pb(II) initial concentration = 10 mg dm^{-3}.

Table 1
The effect of bed depth on breakthrough curve at temperature = 25 ± 0.2°C, pH 4, bed depth of nanomagnetite-loaded PAA hydrogel = 0.25, 0.5, and 1 cm, and flow rate = 1 ml min^{-1}, and Pb(II) initial concentration = 10 mg dm^{-3}

Bed depth (cm)	Flow rate (ml min^{-1})	Inlet lead ion concentration (mg dm^{-3})	t_{total} (min)	m_{total} (mg)	q_{total} (mg)	q_{eq} (mg g^{-1})	Removal (%)
0.25	1	10	170	1.7	1.444	14.44	84.94
0.5	1	10	190	1.9	1.766	8.83	92.95
1	1	10	250	2.5	2.473	6.183	98.92

Table 2
Results of breakthrough curve at different flow rates for adsorption of Pb(II) ions onto nanomagnetite-loaded PAA hydrogel at temperature = 25 ± 0.2°C and pH 4

Flow rate (ml min^{-1})	Bed depth (cm)	Inlet lead ion concentration (mg dm^{-3})	t_{total} (min)	m_{total} (mg)	q_{total} (mg)	q_{eq} (mg g^{-1})	Removal (%)
1	1	10	250	2.5	2.473	6.183	98.92
2	1	10	190	3.8	3.416	8.54	89.89
3	1	10	130	3.9	3.080	7.7	78.97

3.2.3. Effect of initial lead ion concentrations

It was observed that inlet lead ion concentration influenced the shape of breakthrough curves as shown in Fig. 7. With the increase in initial metal ion concentration, breakthrough curves become steeper. At higher concentrations, available binding sites situated on adsorbent surface saturated more quickly, which resulted as early breakthrough time because more adsorption sites are being covered on increasing inlet metal ion concentration. The values are given in Table 3.

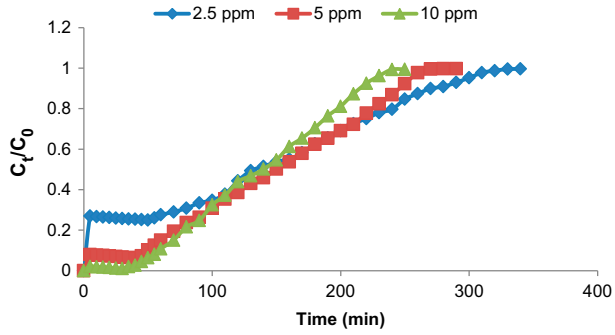

Fig. 7. The effect of inlet adsorbate concentration on breakthrough curve at temperature = 25 ± 0.2°C, pH 4, initial Pb (II) ion concentration = 2.5, 5, and 10 mg dm^{-3}, bed depth = 1 cm, and flow rate = 1 ml min^{-1}.

3.3. Column kinetic study

The design and optimization of a fixed-bed sorption column need to employ some mathematical models, which must be used to describe and predict the experimental breakthrough curves, for possible scale-up of the process. The experimental adsorption data from the microcolumn studies was analyzed using BDST, Thomas, Yoon–Nelson, and Adams–Bohart models to analyze the column performance.

3.3.1. BDST model

The BDST model which is the plot of service time against bed depth at a flow rate of 1 ml min^{-1} was linear (R^2 = 0.981), thus indicating the validity of this model for the present system (shown in Fig. 8). The rate constant (K_a) and sorption capacity of bed (N_0) were calculated from the intercept and slope of BDST plot, respectively. The values of K_a and N_0 are given in Table 4. The rate constant K_a characterizes the rate of solute transfer from the fluid phase to the solid phase. The process parameter bed capacity (N_0) is used to predict the performance of the bed.

3.3.2. Thomas model

The experimental data were fitted with Thomas model to determine maximum capacity of sorption (q_0) and rate constant (K_{Th}). The K_{Th} and q_0 values were calculated from slope and intercept of linear plots of ln [C_0/C_t) − 1] against t at different flow rates, bed heights, and initial metal ion concentrations using values from the column experiments (figures are not

Table 3
Results of breakthrough curve at different inlet adsorbate concentrations for adsorption of Pb(II) ions onto nanomagnetite-loaded PAA hydrogel at temperature = 25 ± 0.2°C and pH 4

Inlet lead ion concentration (mg dm^{-3})	Bed depth (cm)	Flow rate (ml min^{-1})	t_{total} (min)	m_{total} (mg)	q_{total} (mg)	q_{eq} (mg g^{-1})	Removal (%)
2.5	1	1	340	0.850	0.638	1.595	75.06
5	1	1	290	1.450	1.360	3.4	93.79
10	1	1	250	2.5	2.473	6.183	98.92

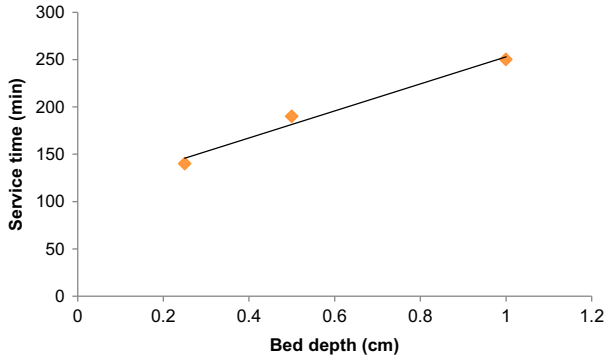

Fig. 8. BDST model of Pb(II) ions adsorption by nanomagnetite-loaded PAA hydrogel at temperature = 25 ± 0.2°C, pH 4, flow rate = 1 ml min^{-1}, and Pb(II) initial concentration = 10 mg dm^{-3}.

Table 4
Calculated constant of bed depth service time equation for adsorption of Pb(II) ions onto nanomagnetite-loaded PAA hydrogel

Adsorbent	N_0 (mg l^{-1})	K_a (l mg^{-1} min^{-1})	R^2
Nanomagnetite-loaded PAA hydrogel	1,428	0.0411	0.981

shown). It can be concluded on the basis of the regression coefficient (R^2) and other parameters that the experimental data fitted well with Thomas model. The model parameters are listed in Table 5. As the concentration increased, the value of K_{Th} decreased, whereas the value of q_0 showed a reverse trend, i.e. increased with increase in concentration. The maximum bed capacity (q_0) decreased with increase in flow rate as well as bed depth. K_{Th} values increased with increase in the flow rate but decreased with increase in bed depth. Similar trend has also been observed for sorption of Cr(VI) using activated weed-fixed-bed column [20].

3.3.3. Yoon and Nelson model

A plot of ln $[C_e/(C_0-C_e)]$ vs. t gave a straight line with slope of K_{YN} and intercept of $-\tau.K_{YN}$. The values of K_{YN}, τ and adsorption capacity q_0 are listed in Table 6. The results show that K_{YN} increased with the increase in concentration, whereas the 50% breakthrough time, τ decreased. Also, the adsorption capacity q_0 increased with increase in initial lead ion concentration and decreased with increase in bed depth and flow rate. The rate constant increased with

Table 5
Thomas model parameters of adsorption of Pb(II) ions onto nanomagnetite-loaded PAA hydrogel at different conditions using linear regression analysis

		Thomas model parameters		
S. No.	Factors	k_{Th} (ml min^{-1} mg^{-1})	q_0 (mg g^{-1})	R^2
1.	Bed height (cm)			
(a)	0.25	3.7	4.489	0.992
(b)	0.5	3	4.11	0.969
(c)	1	2.9	3.544	0.962
2.	Flow rate (ml min^{-1})			
(a)	1	2.9	3.544	0.962
(b)	2	5.6	1.898	0.969
(c)	3	12.3	0.982	0.994
3.	Initial Pb(II) concentration (mg dm^{-3})			
(a)	2.5	5.6	0.894	0.986
(b)	5	4	1.873	0.978
(c)	10	2.9	3.544	0.962

the increase in flow rate but decreased with the increase in bed depth. The time required for 50% breakthrough, τ decreased with increase in flow rate and increased with increase in bed depth. High values of correlation coefficients indicate that Yoon and Nelson model fitted well to the experimental data. For this model, the calculated τ values are quite close to those found experimentally, which indicates that the parameters of the model are similar to those obtained in the experiments.

Table 6
Yoon–Nelson model parameters of adsorption of Pb(II) ions onto nanomagnetite-loaded PAA hydrogel at different conditions using linear regression analysis

		Yoon and Nelson model parameters			
S. No.	Factors	K_{YN} (min^{-1})	τ (min)	q_0 (mg g^{-1})	R^2
1.	Bed height (cm)				
(a)	0.25	0.037	44.89	4.489	0.992
(b)	0.5	0.030	82.2	4.11	0.969
(c)	1	0.014	141.76	3.544	0.962
2.	Flow rate (ml min^{-1})				
(a)	1	0.029	141.76	3.544	0.962
(b)	2	0.028	75.93	3.797	0.976
(c)	3	0.041	39.44	2.958	0.994
3.	Initial Pb(II) concentration (mg dm^{-3})				
(a)	2.5	0.014	143	0.894	0.986
(b)	5	0.020	149.8	1.873	0.977
(c)	10	0.029	141.76	3.544	0.962

3.3.4. Adams–Bohart model

Linear plots of ln (C_t/C_0) against time, t at different bed depths, initial metal ion concentrations, and flow rates were plotted (figures are not shown). Values of K_{AB} and q_{AB} were calculated from the slope and intercept of the linear curves, respectively, and listed in Table 7. Values of K_{AB} increased with increase in bed depth but decreased with increase in flow rate and initial metal ion concentration. However, q_{AB} values decreased for increasing bed depth but increased for increasing flow rate and initial metal ion concentration. Poor correlation coefficients indicate less applicability of this model.

3.4. Desorption studies

Desorption results indicated 99.92% recovery of Pb (II) ions from the surface of the sorbent using 0.1 M HNO_3 in 4 h at 25°C temperature. The results are shown in Fig. 9. The nanomagnetite-loaded PAA hydrogel showed almost the same metal ion adsorption capacity after the repeated regeneration. It may be stated that, in acidic medium, protons compete with Pb(II) ions and displace the maximum amount of adsorbed lead. Hence, ion-exchange mechanism is important in connection with adsorption–desorption process for adsorbent.

3.5. Mechanism of uptake

The nanomagnetite-loaded PAA hydrogel contains carboxyl and amide groups as confirmed by FTIR analysis that are responsible for binding the toxic Pb(II) ions on the surface. The proposed mechanism of binding the Pb(II) ions on various sites available at adsorbent surface (Fig. 10) may be explained as follows.

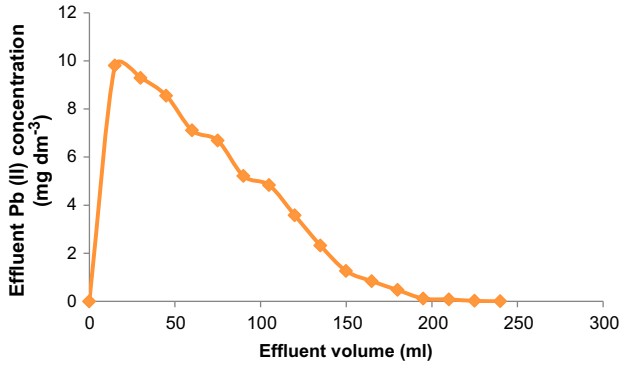

Fig. 9. Desorption studies of Pb(II) ions using 0.1 M HNO_3 solution with Pb(II) adsorbed fix-bed microcolumn of nanomagnetite-loaded PAA hydrogel at temperature = 25 ± 0.2°C, flow rate = 1 ml min^{-1}, and bed depth = 1 cm.

(1) Carboxylate groups (–COO^-) of acrylic acid moiety of copolymer interact with Pb(II) ions.
(2) Pb(II) ions coordinate with the electron-rich nitrogen of amide group of acrylamide moiety of copolymer.
(3) Pb(II) ions co-ordinate with the electron-rich nitrogen of amide group of N,N′-methylene-bis-acrylamide moiety (cross-linking agent).
(4) In addition, within the copolymer matrix, these Pb(II) ions may coordinate with the electron-rich oxygen of magnetite nanoparticles.

Table 7
Adams–Bohart model parameters of adsorption of Pb(II) ions onto nanomagnetite-loaded PAA hydrogel at different conditions using linear regression analysis

			Adams–Bohart model parameters		
S. No.	Factors	K_{AB} (l mg^{-1} min^{-1})	q_{AB} (mg l^{-1})	q (mg g^{-1})	R^2
1.	Bed height (cm)				
(a)	0.25	1.4	4.046	5.664	0.876
(b)	0.5	1.3	3.089	2.935	0.841
(c)	1	1.8	1.942	1.214	0.847
2.	Flow rate (ml min^{-1})				
(a)	1	1.8	1.942	1.214	0.847
(b)	2	1.2	2.982	1.416	0.857
(c)	3	1.4	2.85	0.926	0.901
3.	Initial Pb(II) concentration (mg dm^{-3})				
(a)	2.5	2	0.785	0.667	0.970
(b)	5	2	1.225	0.888	0.901
(c)	10.	1.8	1.942	1.214	0.847

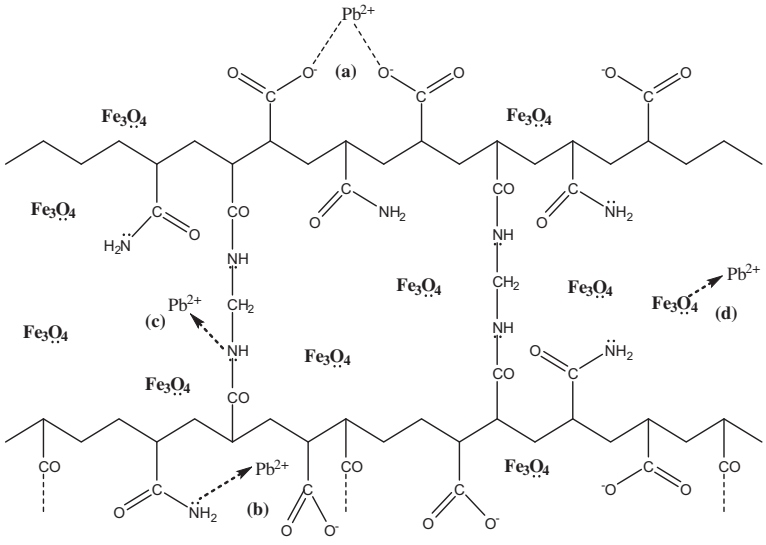

Fig. 10. Scheme of mechanism of Pb(II) ions uptake by nanomagnetite-loaded PAA hydrogel through co-ordination with (a) carboxylate groups of acrylic acid moiety, (b) electron-rich nitrogen of amide group of acrylamide moiety, (c) electron-rich nitrogen of amide group of N,N´-methylene bis acrylamide moiety (cross linking agent), and (d) electron-rich oxygen of magnetite nanoparticles.

3.6. Mechanism of industrial uptake

The efficiency of the nanomagnetite-loaded PAA hydrogels for the removal of toxic lead ions was tested with a metal-polishing industrial wastewater sample. The optimum conditions for removal of lead ions by nanomagnetite-loaded PAA hydrogel in a column system have already been described in the experimental part. The amount of lead ions present in sample (before and after adsorption) was determined by atomic absorption spectrometer. Initially, the concentration of copper ion was found to be 9.5124 mg dm^{-3} in effluent water. The breakthrough curve of column study is shown in Fig. 11. The results were in good agreement with those obtained from column experiments conducted for lead ions removal in synthetic wastewater samples. 98.21% removal of lead was obtained in column adsorption study.

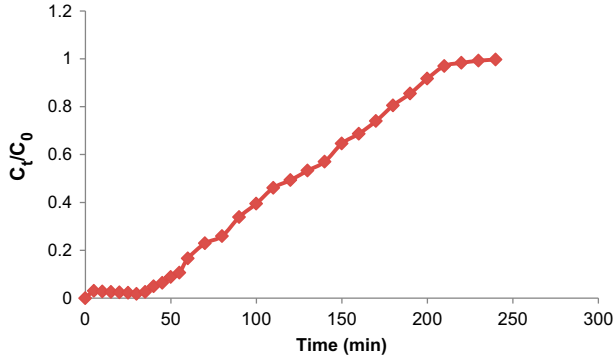

Fig. 11. Breakthrough curve for adsorption of lead onto nanomagnetite-loaded poly (acrylamide-co-acrylic acid) hydrogel at bed height = 1 cm, flow rate = 1 ml min^{-1}, pH 4, and temperature = 25 ± 0.2°C.

4. Conclusion

The adsorbent "nano magnetite loaded PAA hydrogel" has been found to be an effective, efficient, and an inexpensive adsorbent for Pb(II) removal from aqueous solution as well as effluent water. The effects of bed depth, inlet feed concentration, and flow rate on Pb(II) ion adsorption were investigated and the experimental breakthrough curves were obtained. The experiments were performed at 1 ml min^{-1} flow rate, 1 cm bed depth, and 10 mg dm^{-3} inlet lead ion concentration at pH 4. It was observed that equilibrium metal uptake (q_0) increased with increase in flow rate and inlet lead ion concentration and decreased with increase in bed depth. Both breakthrough point and exhaustion time increased with increase in bed depth and inlet lead ion concentration and decreased with increase in flow rate. Thomas, Yoon–Nelson, and Adams–Bohart kinetic models were used to describe the column adsorption kinetics. The experimental breakthrough curve was compared satisfactorily with

the breakthrough profile calculated by Thomas and Yoon–Nelson method. The calculated column parameters could be scaled up for the design of fixed-bed columns for effective and efficient removal of toxic metal ions from water.

Acknowledgments

The authors would like to express thanks to the Department of Atomic Energy, BRNS-BARC, Mumbai, INDIA for providing financial assistance. Authors are also grateful to UGC-DAE Consortium for Scientific Research, Indore for FTIR and AFM analysis, and AIIMS, New Delhi, India for TEM analysis.

References

[1] M. Singanan, Removal of lead (II) and cadmium (II) ions from wastewater using activated biocarbon, Sci. Asia 37 (2011) 115–119.
[2] N.T. Abdel-Ghani, M. Hefny, G.A.F. EI-Chaghaby, Removal of lead from aqueous solution using low cost abundantly available adsorbents, Int. J. Environ. Sci. Technol. 4(1) (2007) 67–73.
[3] S.H. Jang, B.G. Min, Y.G. Jeong, W.S. Lyoo, S.C. Lee, Removal of lead ions in aqueous solution by hydroxyapatite/polyurethane composite foams, J. Hazard. Mater. 152(3) (2008) 1285–1292.
[4] R. Naseem, S.S. Tahir, Removal of Pb(II) from aqueous/acidic solutions by using bentonite as an adsorbent, Water Res. 35(16) (2001) 3982–3986.
[5] H. Sulaymon Abbas, E. Ebrahim Shahlaa, J. Al-Musawi Tariq, M. Abdullah Sama, Removal of lead, cadmium and mercury ions using biosorption, Iraqi J. Chem. Pet. Eng. 11(2) (2010) 1–13.
[6] S.M. Al-Garni, Biosorption of lead by Gram-ve capsulated and non-capsulated bacteria, Water SA 31(3) (2005) 345–350.
[7] J.O. Esalah, M.E. Weber, J.H. Vera, Removal of lead, cadmium and zinc from aqueous solutions by precipitation with sodium di-(n-octyl) phosphinate, Can. J. Chem. Eng. 78(5) (2000) 948–954.
[8] E. Erdem, N. Karapinar, R. Donat, The removal of heavy metal cations by natural zeolites, J. Colloid Interface Sci. 280(2) (2004) 309–314.
[9] Y.S. Ho, J.C.Y. Ng, G. McKay, Removal of lead(II) from effluents by sorption on peat using second-order kinetics, Sep. Sci. Technol. 36 (2001) 241–261.
[10] H.G. Park, T.W. Kim, M.Y. Chae, I.-K. Yoo, Activated carbon containing alginate adsorbent for the simultaneous removal of heavy metals and toxic organics, Process Biochem. 42 (2007) 1371–1377.
[11] W.S. Wan Ngah, C.S. Endud, R. Mayanar, Removal of copper(II) ions from aqueous solution onto chitosan and cross-linked chitosan beads, React. Funct. Polym. 50(2) (2002) 181–190.
[12] B. George, V.N. Rajasekharan Pillai, B. Mathew, Effect of the nature of the crosslinking agent on the metal-ion complexation characteristics of 4 mol% DVB- and NNMBA-crosslinked polyacrylamide-supported glycines, J. Appl. Polym. Sci. 74 (1999) 3432–3444.
[13] B. Mathew, V.N.R. Pillai, Polymer–metal complexes of amino functionalized divinylbenzene-crosslinked polyacrylamides, Polymer 34 (1993) 2650–2658.
[14] D. Lindsay, D.C. Sherrington, J.A. Greig, R.D. Hancock, Copper-selective chelating resins. I. Batch extractions, React. Polym. 12(1) (1990) 59–73.
[15] B.R. Green, R.D. Hancock, The role of matrix effects on selectivity in ion exchange resins, Hydrometallurgy 6 (1981) 353–363.
[16] A. Tiwari, N. Sharma, Efficiency of superparamagnetic nano iron oxide loaded poly (acrylamide-co-acrylic acid) hydrogel in uptaking Pb^{2+} ions from water, Int. Res. J. Environ. Sci. 1(5) (2012) 6–13.
[17] Z. Aksu, F. Gönen, Biosorption of phenol by immobilized activated sludge in a continuous packed bed: Prediction of breakthrough curves, Process Biochem. 39 (2004) 599–613.
[18] V.C. Taty-Costodes, H. Fauduet, C. Porte, Y.S. Ho, Removal of lead (II) ions from synthetic and real effluents using immobilized *Pinus sylvestris* sawdust: Adsorption on a fixed-bed column, J. Hazard. Mater. 123 (2005) 135–144.
[19] V. Sarin, T.S. Singh, K.K. Pant, Thermodynamic and breakthrough column studies for the selective sorption of chromium from industrial effluent on activated eucalyptus bark, Bioresour. Technol. 97 (2006) 1986–1993.
[20] S.S. Baral, N. Das, T.S. Ramulu, S.K. Sahoo, S.N. Das, G.R. Chaudhury, Removal of Cr(VI) by thermally activated weed *Salvinia cucullata* in a fixed bed column, J. Hazard. Mater. 161 (2009) 1427–1435.